American Journal of Technology Advancement Vol. 3, No.1 (Jan, 2026),
E-ISSN: 2997-9382
American Journal of Technology Advancement
https://semantjournals.org/index.php/AJTA

| Research Article

Check for updates

Improving Thermal Performance of Plate-Fin Heat Sinks Using Baffles: A Computational and Experimental Investigation

Murtadha Saeed Mohammed
Mechanical Engineering Department, University of Misan, Misan, Iraq
E-mail: murtadha.saeed@uomisan.edu.iq

Abstract

The results of the extensive thermal-hydraulic performance investigation carried out in this study were determined by using a combination of computational and experimental methods to investigate the thermal-hydraulic performance of the Plate-Fin Heat Sink (PFHS), which has been enhanced with transverse copper baffles. The investigation was conducted using a Reynolds number (Re) range of 1013 to 3832 under a variety of (80-120 W) heat loads to assess the effectiveness of modulating the flow for the purpose of enhancing heat transfer. In order to validate the CFD model with the experimental data, three-dimensional Computational Fluid Dynamics (CFD) modelling was used with the standard k-epsilon turbulence formulation. Validation of the CFD model resulted in an average deviation of 4.75% from the experimental data, indicating that the CFD model provided an accurate representation of the experimental results. The results of the investigation indicate that the copper baffles significantly disrupt the thermal boundary layer and induce flow splitting, and therefore function as effective vortex generators. As a result of the baffled configuration, the maximum thermal resistance was reduced by 12.9%. The average enhancement in Nusselt number (Nu) compared to the unbaffled PFHS was 7.7% - 8.9%. Through testing, researchers showed a steady increase in heat transfer coefficient (HTC) for an experimental fluid as their Reynolds number increased from 1013 to 3832 because the increase in HTC resulted from the suppression of the thermal boundary layer and the improvement of fluid mixing.

Keywords: Plate-Fin Heat Sink, Passive Enhancement, Baffles, CFD Validation, Thermal Resistance, Electronic Cooling

This is an open-access article under the CC-BY 4.0 license

1. Introduction

Fast-advancing industrial systems generate large amounts of heat, leading to an increasing demand for energy. Devices are becoming increasingly miniaturized, making it imperative to provide adequate cooling capabilities to minimize heat build-up in order to avoid degrading the performance of & maintain the life of these devices [1], [2]. As a result of this and other factors, much attention has been placed on finding ways to improve heat sinks, with Plate-Fin Heat Sinks

(PFHS) representing a tremendous advantage in terms of cost and performance [3], [4]. However, increasing thermal loads on conventional PFHS design pose a problem that is increasing as the size of devices becomes smaller, as this is due to the continuous formation of thermal boundary layers and which ultimately limits the efficiency of heat transfer [5]. Increasing the amount of air being directed over PFHS by utilizing active cooling systems may help to reduce the thermal load from device usage; however, this leads to increased energy usage & acoustic noise, making this solution an unsustainable approach to the problem in the long run [6].

Research has recently focused on using passive enhancement techniques like baffle systems to control fluid flow without applying any additional mechanical or electrical energy [7], such as a passive means of modulation. Baffles are effective at improving the efficiency of heat transfer because they disturb the laminar layers of flow and promote mixing via turbulent flows, resulting in increased convective/radiative transfer rates [8]. However, this disruption leads to hydraulic losses; therefore, a trade-off exists between the increased efficiency and the decreased pressure. Although there is some published work related to fins, very little of this prior work addresses the validation of computational fluid dynamics (CFD) models and experimental measurements of the thermal-hydraulic performance of baffled distributions. Thus, this research will fill this void through experimental and numerical investigations of the thermal-hydraulic characteristics of a baffled PFHS. The specific aims of this investigation will be to study how the interaction between Reynolds number, thermal resistance, and pressure loss can affect the system performance and generate validated data to support the development of optimized energy-efficient systems for managing thermal load.

Literature Review

The thermal management of power electronics, electronic systems, and industrial heat exchangers has become a paramount challenge in modern engineering, driven by the relentless trend toward miniaturization and increasing power densities. A primary source of heat removal for electronic equipment and power electronics, Plate-Fin Heat Sinks (PFHS) are the simplest and most dependable methods of removing heat; however, the creation of continuous thermal boundary layers limits the heat transfer characteristics of PFHS. Baffle placement has been developed as a strategy for increasing the thermal performance of PFHS; hence, this literature review presents approximately 40 computational and experimental investigations regarding baffle configurations, the methods by which baffles enhance thermal performance, and the trade-offs between thermal efficiency and hydraulic resistance between the years 2007 and 2025.

70% of existing research on swirling jets is computational, using turbulent (Re=20000) or laminar (Re=0.1) and up to Re=46000 (high-speed) as flow types. Even though 70% of today's research is computationally verified (with few exceptions), the biggest limitation to today's research is that many of the computational simulations will never be experimentally verified by an experimental facility. Xin Cao et al [10] have published hybrid experimental and computational methods, producing experimental results that are within eight per cent of CFD results. These experimental studies illustrate the importance of experimental validation and provide evidence that experimental validation is one of the methodologies utilized in the current study.

Three primary methods by which baffles increase heat transfer are: boundary layer disruption, vortex generation, and jet impingement. Baffle-type devices create turbulence as a result of boundary layer destruction from baffles (H. Ameur et al. [11]), as vortex generation occurs at the edges of structured baffles (Kang et al. [12]). The improvement in heat transfer performance of a design using notches can be attributed to the addition of multiple jets impinging on the surface (Phila et al. [13]). In this study, it was planned to utilize these effects to achieve the maximum heat transfer performance possible in a specific volume.

The reported improvements in performance vary widely, from 509% as reported by Y. Menni et al. [15] using baffles of the "V" shape; however, those same gains were accompanied by hydraulic penalties that decreased thermal enhancement factor (TEF) in turbulent waterflow applications below levels of 2.0, thereby establishing a clear relationship between the design of the unit for cooling capability and the amount of pumping energy required to pump through the unit (the Profit Factor). Therefore, the purpose of this continuing investigation will be to derive the optimum design to create the maximum Profit Factor for cooling performance. In the literature, researchers have noted convergence to particular optimum geometries during the studies done to date. V-shape baffles oriented at a 45˚ angle have been shown to provide the best aerothermal performance. H. Ameur et al. [11] have demonstrated that elliptical holes offer a reduction in drag of approximately 63.4% relative to circular holes, thereby showing that small geometric changes (e.g., the different pitch-to-baffle ratios being studied) are necessary to minimize hydraulic losses through the unit.

The capability of baffled PFHS to adapt to many industries is demonstrated by the fact that in non-electrical industries, Y. Tsay et al. [17] have demonstrated nearly 85% overall (Nusselt) improvements in the cooling of electrical components, and I. T'Jollyn et al. [18] have shown that a baffled PFHS will produce a higher cooling effect on electric vehicles compared to pin fins. These findings support the continued development of optimized and manufacturable designs for multiple engineering applications. Optimization has been identified as an essential feature of improving solar air heating performance, as illustrated by the work of Ramadhani Bakari et al. [19] who identified the baffle count necessary to improve thermal efficiency without significantly increasing the pressure drop.

While substantial research has been conducted to investigate the issue, there still exist serious deficiencies in our understanding. First, many studies do not consider the constraints faced by manufacturers or the economic implications of producing complex geometries. Second, no multi-scale optimization has been attempted to date that looks at micro-geometry together with macro-system characteristics. Lastly, and perhaps most importantly, most studies have relied solely on computational fluid dynamics (CFD) with little or no experimental corroboration. This research will attempt to fill these deficiencies by using both computation and experimentation to validate the optimization process, thus providing accurate predictions regarding the relationship between the thermal resistance and pressure drop of energy-efficient thermal management systems.

2. Methodology

This section provides information on the geometry of the heat sink models, the test equipment employed to confirm the results, and the computer simulation model used in the numerical study.

2.1. Physical Model and Geometry

The Plate-Fin Heat Sink (PFHS) was made from the Aluminium 1050 alloy for its thermal conductivity (k≈229 W/m·K) and manufacturing simplicity. The PFHS is rectangular in shape (overall dimensions = 92x100×31 mm(W×L×H)). As illustrated in Figure 2, the PFHS consists of an array of 10 fins extending from a 6 mm thick base plate in a parallel vein in the direction of flow (100 mm long). The use of copper baffle plates was implemented in the flow channels to enhance the thermal transfer rate, as shown in Figure 3. The arrangement of these baffle plates consists of five transverse rows across the top of the fins and was held by metal rods to create a cross-flow obstruction to disrupt the thermal boundary layer and enhance mixing. See Figure 1.

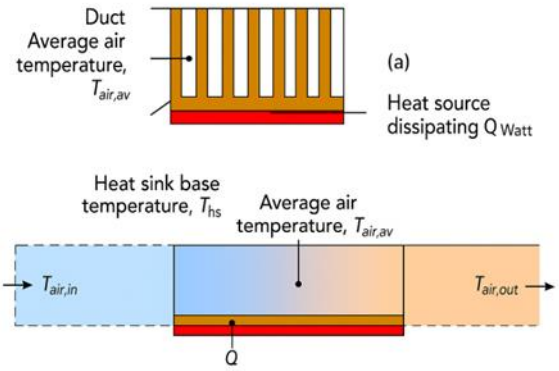

Figure 1. General arrangement of wind tunnel setup.

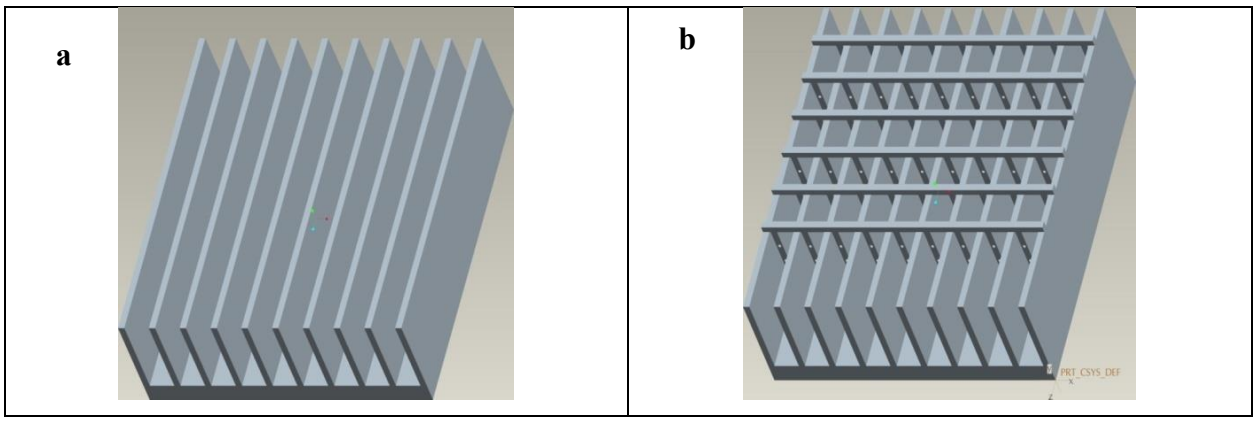

Figure 2. a. Heat sink with plate fins but no baffle plate connection, and b. Plate fin heat sink with a connection for the baffle plate.

Table 1. Geometric specifications of the Plate-Fin Heat Sink.

Characteristic	With baffles	Without baffles
Heat sink width, W(mm)	92	92
Heat sink depth, H(mm)	31	31
Heat sink length (mm)	100	100
Fin width, W(mm)	2	2
Fin length, L (mm)	25	25
Fin pitch, P (mm)	8	8
Base plate thickness (mm)	6	6

2.2 Instrumentation and Test Apparatus

A custom-built, open-circuit wind tunnel was used to conduct the experimental investigation to create a controlled environment for free convection (forced convection). A schematic drawing of the experimental apparatus has been provided (Figure 3). The experimental device is constructed from three principal components: the inlet section (settling chamber), the testing section, and the discharge section.

2.2.1 Airflow System

The airflow in this tunnel was created by a 2.2 kW centrifugal blower located at the end of the TMO (suction mode). The blower created less turbulence in the working section, allowing for better measurement of forces acting on a body. Air passed through a straight rectangular duct with

internal dimensions of 120 mm x 150 mm, then through a honeycomb flow straightener at the entrance of the working section. To provide a uniform velocity profile and reduce the formation of large-scale eddies, the inlet of the honeycomb flow straightener had been designed using analytical modelling, as shown in Section 2. The velocity of air entering the working section was controlled by a voltage regulator applied to the blower motor and was measured upstream of the working section with a hot-wire anemometer, reading an accuracy of ±0.1 m/s, located 50 mm upstream of the working section.

2.2.2 Heating and Test Section

The Plate-Fin Heat Sink (PFHS) was installed in the bottom wall of the test section in a flush-mounted position. In order to emulate the heat generated by an electronic component, a resistive heater (with dimensions equal to those of the HSF's base) was placed on top of the PFHS and secured to it using a thin film of High-Conductivity Thermal Interface Material (TIM). This film was used to reduce the thermal contact resistance between the heater and the heat sink. The resistive heater was powered by a precision DC Power Supply (BEETECH DC-3005), which allowed for precise control of both the voltage and current supplied to it. The test section was insulated with 20 mm of glass wool for the purpose of maintaining an adiabatic boundary condition and directing all heat flux into the airstream.

2.2.3. Data Acquisition

In the section of Data Acquisition, a high-quality 12-channel data logger was used to assemble the data for this research project. The following describes how temperatures were measured with a K-type thermocouple (with a precision of 0.1 °C) in various areas on the heating and cooling pipe surfaces:

The Tin measurement was taken with a single thermocouple at the pipe inlet, and the Tout measurement was performed with three thermocouples to average the temperatures at the pipe outlet. The Tbase temperature measurements were obtained from three thermocouples that were installed into the base of the heat sink and set to a depth of 1 mm in order to provide a representation of the temperature distribution across the surface of the base. To measure the static pressure drop across the heat sink, the P values were obtained with the use of a digital differential pressure transmitter connected to two static pressure taps, which were located at a distance of 50 mm from the heat sink in both directions.

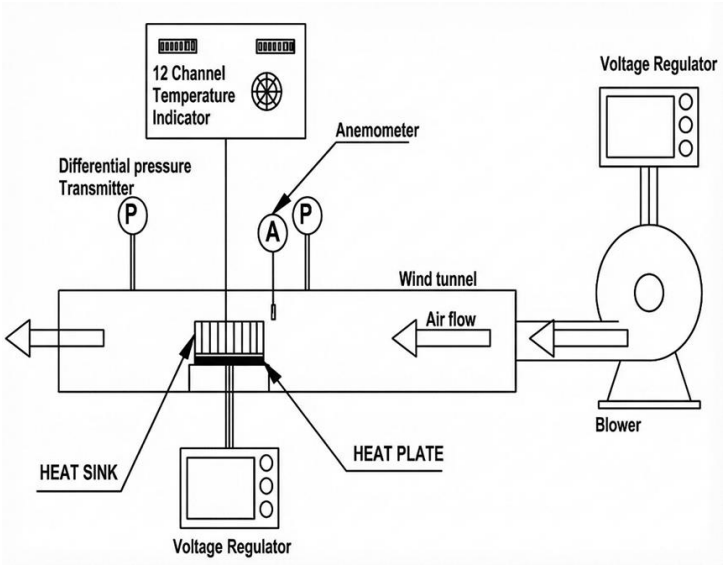

Figure 3. Schematic diagram of experimental setup.

2.2.4 Production of Heat Sinks

A PFHS is a heat sink manufactured out of Aluminum 1050 by way of CNC machines. Copper was used to create baffle plates for the baffles (which are mounted onto a certain surface). Firstly, they were welded to copper studs along the top of the fins and additionally secured to the fins on the upper side, as shown in Figures 5, which display these types of heat sinks with locations denoting where the thermocouples should be installed and an attached baffle assembly.

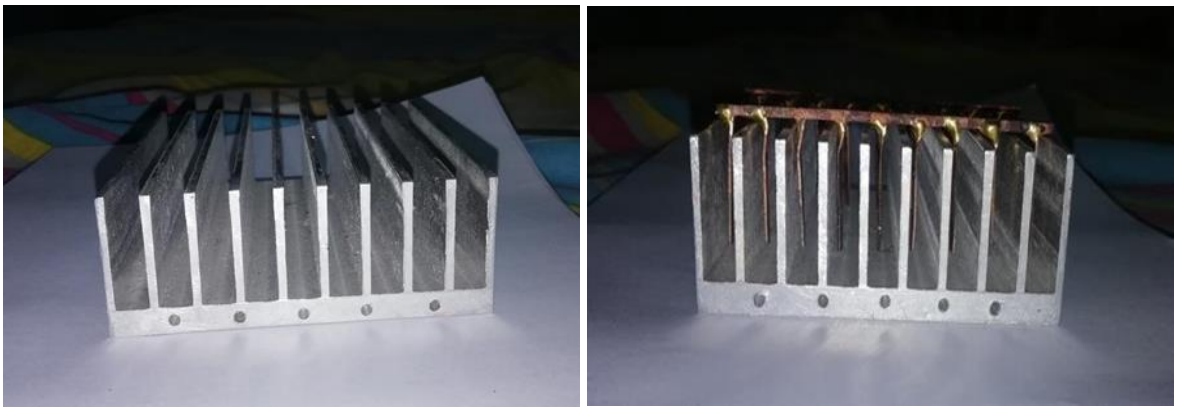

Figure 4. Fabricated view of the Heat sink with the thermocouple location.

2.2.5 Test Apparatus

The wind tunnel utilized for this experiment was an open-circuit design. The test section is a rectangular duct with a hydraulic diameter, Dh, determined from the cross-sectional area, Ac, and the wetted perimeter, P, according to the following equation:

$$D_h = \frac{4A_c}{P} \quad (1)$$

In order to ensure accurate measurement, the heat sink was placed within the location of the fully developed flow region. Therefore, to determine where the flow develops, the required hydrodynamic entrance length, L_h, was established. The hydrodynamic entrance lengths for certain ranges of Reynolds numbers, for laminar and turbulent flow, were estimated using equations 1 and 2, respectively.

$$L_{h,laminar} \approx 0.05 \cdot Re \cdot D_h \quad (2)$$

$$L_{h,turbulent} \approx 4.4 \cdot D_h \cdot (Re)^{1/6} \quad (3)$$

According to these computations, the velocity of the air was measured at a position in the test section that was approximated to be located 500 millimetres behind the output of the blower. In this position, it could be confirmed that the viscous boundary layers were, in this region of free space, fully established.

2.2.6 Equipment Location for Measurement

- Temperature: K-type thermocouples were utilized to measure the thermal profile; specifically, four sensor locations within the duct inlet, and four sensor locations within the duct exit for measuring air temperature, three sensor locations positioned inside the heat sink base for measuring surface temperature, as well as an ambient atmospheric sensor.
- Pressure: Static pressure taps were drilled into both the heat sink inlet and outlet walls. These birdcage shapes were then connected via tubes to a U-tube manometer in order to determine pressure loss.

- Power: The power supplied to the heat sink was regulated through a variable autotransformer (Voltage Regulator), then monitored with a digital wattmeter.

2.2.7 Experimental Procedure

The following steps were followed during the experimental trials carried out under steady state conditions:

- The PFHS was firmly secured on the heater platform of the test section.
- The blower was turned on, and an adjusted voltage regulator was set to establish an appropriate air speed.
- The heater was turned on to achieve a specific heat flux (upwards of 45 kW/m^2).
- The system was allowed to stabilize for a minimum of 15 to 30 minutes after turning on, and a steady state condition was achieved when the temperature measurements were constant through time.
- When the system attained a steady condition, temperature readings, inlet and outlet temperatures of the air, and pressure drop and air speed were measured.
- This procedure took place for a total of 15 sets (for both baffled and unbaffled configurations) by changing the heat input and air speed (as contained in the table provided for the parametric study).

2.3 Data Reduction and Mathematical Formulation

The Control Volume Method was used to determine the thermal performance, with the thermal resistance being represented by R_{th}. By using this method, we were able to find the total R_{th} by using the following equation:

$$R_{th} = \frac{T_{avg} - T_{amb}}{Q} \quad (4)$$

T is the average temperature, which averages eight temperature readings at different heat sink locations. Q is the heat sink's heating power. R_{th} is the heat sink's thermal resistance. The temperature of the cooling air near the thermosphere. The method used to determine the Reynolds number is

$$Re = \frac{VD}{V} \quad (5)$$

The hydraulic diameter is indicated by D, the cooling air velocity by V, and the air's kinematic viscosity by v.

The hydraulic diameter, D, is determined

$$D = \frac{2(B - Nt)}{N - 1} \quad (6)$$

Where N is the number of fins, t is the thickness of the fins, and B is the heat sink breadth.

h, the heat transfer coefficient on average is computed using

$$h = \frac{Q}{A_h(T_{base} - T_{in})} \quad (7)$$

And can be calculated by the following equation:

$$A_h = \frac{2H_h BL}{\delta} \quad (8)$$

Nusselt number (Nu)

$$Nu = \frac{hD}{k_a} \quad (9)$$

To measure its use, Sansoucy et al. introduced the Coefficient of Expansion (COE), which may be expressed as

$$COE = \frac{Nuwb}{Nuwob} \quad (10)$$

Here, NuWB is denoted as a Nusselt number with baffles, and NuWOB is denoted as a Nusselt Number without baffles.

Sparrow et al. defined in their study that the calculation of heat sink fluid pumping power is defined as

$$P = (mp)\Delta p = U_{in} A_p \Delta p \quad (11)$$

$$A_p = H\delta(N-1) \quad (12)$$

where N is the number of fins, δ is the fin spacing, and H is the fin height.

2.3.1 Uncertainty Measurement in Heat Sink

A number of instruments are available to measure heat sink temperature to calculate its performance, and these instruments work based on electronic effects. The temperature-measuring instruments, K-type thermocouples, and thermistors can be utilized for measurement in Heat sinks. The wind tunnel's differential pressure and flow velocity are also measured using a manometer, much like in pressure measurement. The voltage and amps displayed in the voltmeter and ammeter are multiplied to determine the input heat power. Reynolds number (Re) is dependent upon diameter, viscosity (μ), density (ρ), and velocity (V). (D) of the liquid.

2.3.2 Overall Uncertainty

Robert J Moffat defined the equations below to calculate pressure and temperature gradient uncertainty.

$$(UR)0.95 = \{(BR)^2 + (tSR)^2\}^{1/2} \quad (13)$$

R is the range surrounding the mean value, and the exact value is expected to endure.

2.3.3 Bias Limit

The overall methodical uncertainty on the helicity portion is calculated by totaling all the uncertainties from the apiece area expressed above in quadrature. The bias boundary influences all measured values, which are directly proportional to its sensitivity coefficient (If the experimentally calculated value is Xi, R is the partial derivative of Xi, then BR is calculated as mentioned in the equation.

$$B_R = \left\{\sum_{t=1}^{N} \left(\frac{\partial \mathrm{R}}{\partial X_t} B_t\right)^2\right\}^{1/2} \quad (14)$$

Bi - Uncertainty in bias limit

BR - Overall uncertainty in the result

Xi- R's partial derivative concerning Xi multiplied by the variable's uncertainty interval.

N- Number of repeated observations of each measurement

2.3.4 Precision Index

The precision index is the magnitude of random errors in a successive interpretation from an experimental measurement. The random errors are inversely proportional to its precision index. The random error is minimal if the precision index is high. The Gaussian law includes the precision index parameter, which is influenced by all measurement values in an experiment. It is calculated by:

$$S_R = \left\{\sum_{t=1}^{N}\left(\frac{\partial \mathrm{R}}{\partial X_t}S_t\right)^2\right\}^{1/2} \quad (15)$$

SR- Precision index of the result, SR

Xi - A partial derivative of R relative to Xi multiplied by the variable's uncertainty interval.

N- Number of repeated observations of each measurement Bi -Uncertainty in precision index

2.4 Numerical Simulation Methodology

In order to better understand the airflow physics of the experimental testing, three-dimensional numerical modelling was performed using the commercially available Ansys Cfx 14.0 Computational Fluid Dynamics (CFD) software.

2.4.1. Model Equations and Numerical Model Attributes

The numerical model consisted of a steady-state incompressible flow solution of the Navier-Stokes mass conservation (continuity), momentum conservation, and energy conservation equations. The airflow was assumed fully developed with no gravitational forces. The maximum velocity of air corresponds to a Mach number much less than 0.3 (V ≈5 m/s); therefore, the compressible nature of the airflow was ignored. The turbulence model used in the simulation was the standard k-ϵ model, which has been shown through numerous studies to be robust and computationally affordable for the prediction of the turbulent flow characteristics of heat sink flow channels. The governing exponential equations are presented here:

Continuity Equation: $\nabla \cdot (\rho\vec{U}) = 0$

Momentum Equation: $\nabla \cdot (\rho\vec{U}\vec{U}) = -\nabla P + \nabla \cdot (\mu\nabla\vec{U}) + S_M$

Energy Equation: $\nabla \cdot (\rho\vec{U}C_pT) = \nabla \cdot (k\nabla T) + S_E$

Where ρ: is density, $\vec{U}$: is the velocity vector, P: is pressure, μ: is dynamic viscosity, C_p: is specific heat capacity, and k: is thermal conductivity.

2.4.2. Computational Domain and Boundary Conditions

To model the experiment, the computational domain mirrors the experimental set-up, with the solid domain (aluminum heat sink and copper baffle) and the fluid domain (air moving through the duct). The computational domain has four boundary conditions, which are:

Inlet: A uniform velocity inlet that matches the experimental air velocities was used.

Outlet: A pressure outlet at a gauge pressure of 0 Pa (1 atm) was used.

Heat Source: A constant heat flux was applied at the base of the heat sink as the heat source.

Walls: The duct walls had an adiabatic, no-slip condition, and the heat transfer between the fluid and the solid was treated as coupled.

2.4.3. Mesh Generation

An unstructured tetrahedral mesh was generated to represent the complex geometry of the baffled heat sink, as shown in Figure 5. The use of tetrahedral elements was chosen due to their ability to adapt to the complex shape of the baffled heat sink. The mesh is finer at the fin walls and baffle regions to accurately capture the boundary layer gradients.

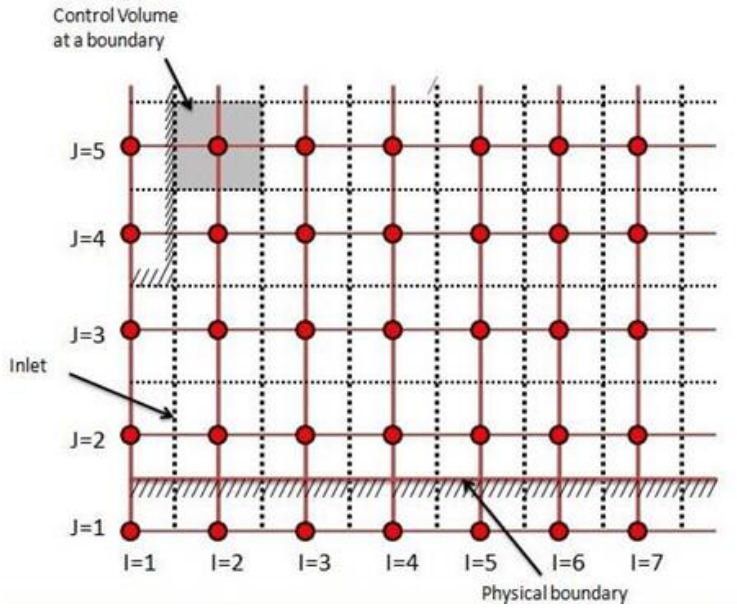

Figure 5. Principle of CFD Grid Generation.

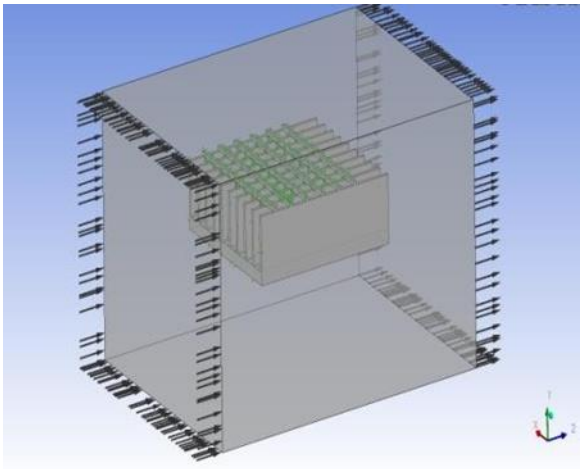

Figure 6. Solid model of Plate fin heat sink with baffles.

Analysis of Meshing Resolution

To determine that the results of the numerical study could be replicated with different sizes of mesh elements, an analysis of grid sensitivity was performed. The grids which were analyzed were: 525601 elements, 657894 elements, 769417 elements, and 854684 elements. The average base temperature was selected as the dependent variable for comparisons between grids. Figure 10 provides the comparisons for grid element sizes. It may be seen that for the grids with 769417 elements and 854684 elements, the difference in temperature was found to be less than 0.15%. Therefore, the optimal grid for further studies was the grid that contained 769417 elements (155091 nodes), as it provided both an acceptable level of accuracy compared with the other grids but also provided value for money from an operational perspective.

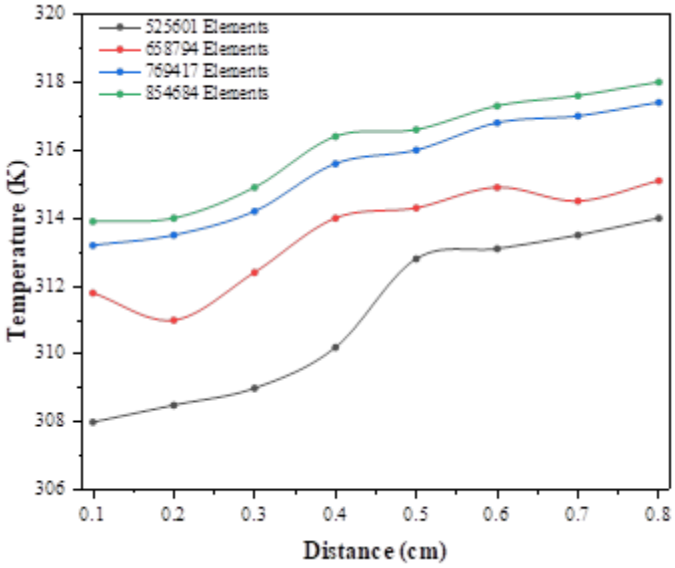

Figure 7. Temperature distribution variation with distance.

3. Results and Discussion

This section reports on both experimental and computational data on Plate-Fin Heat Sink (PFHS) thermal performance. The analysis covers how Reynolds number and heat input affected PFHS thermal resistance, and how PFHS thermal performance was improved through the use of baffle configurations.

3.1. Impact of Reynolds Number on Resistance to Heat Transfer

Using various Reynolds numbers (between 1013 and 3832) and different amounts of heat applied to Plate-Fin Heat Sinks (from about 80 W to about 120 W), the thermal resistance for these types of sinks was found to display a very distinct inverse reaction. Rth decreased considerably as the airflow velocity increased for both types (with and without baffles). The decrease in Rth is attributed to a reduction in the thickness of the thermal boundary layer along with enhanced convective heat transfer. Somewhat lower thermal resistance also occurred with an increase in the amount of heat that could be added to PFHS. This effect is due to fluid properties that vary based on the temperature of the fluid. In every case, the comparison of baffled versus unbaffled configurations indicates that adding baffles consistently improves performance over baseline configurations. At the lowest flow rates, Re = 1013, and at the highest heat outputs of 120 W, baffles could reduce thermal resistance by an average of 12.1% compared to no baffles. This level of improvement, at its highest value of 12.9%, can generally be attributed to an increase in the effectiveness of the baffles on the way they can help break up the formation of a boundary layer as well as inducing vortex flows, mixing cool core air with hot fin surfaces.

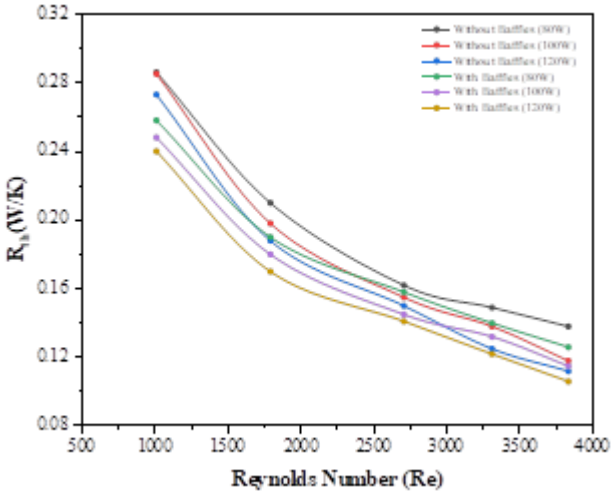

Figure 8. Variation of Thermal Resistance vs. Reynolds Number at various heat inputs (80 W, 100 W, and 120 W).

3.2. A Comparative Analysis of Nusselt Number Augmentation

It was found that all configurations had a good positive relationship between the Reynolds Number (1013-3832), which is indicative of increasing turbulence level and decreasing thickness of laminar sublayer, and the Nusselt Number (Nu), which is representative of overall convective heat transfer performance. Baffled Plate-Fin Heat Sink (PFHS) configurations had steadily better performance than unbaffled configurations; at Re = 3832 and a heat load of 100 W, for example, the Nusselt Number increased from 71.5 to 88.5 due to the disruptive influence of the baffle(s) on the thermal boundary layer and resulting secondary flow vortices, which improved fluid mixing. Baffled designs provided an average Nusselt Number increase of 7.7%, 8.9%, and 6.4% for heat loads of 80 W, 100 W, and 120 W, respectively, supporting the use of geometric modification as an effective means by which to enhance thermal performance in size-constrained applications.

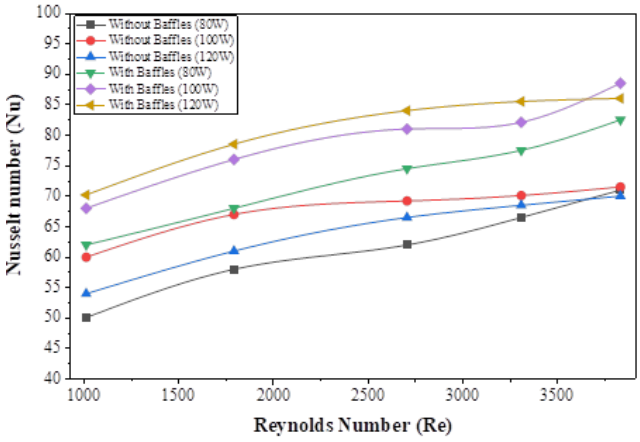

Figure 9. Variation of Nusselt Number vs. Reynolds Number for baffled and unbaffled configurations.

3.3. Effect of Reynolds Number on Thermal Performance

Data from both experiments and CFD simulations agree with each other. There was also an observable linear relationship between the value of the convective heat transfer coefficient (h) and Reynolds Number (Re) due to the dominance of inertial forces over viscous forces at increased flow rates from 1013 to 3832 at all heat loads (80 to 120 watts) tested.

Increasing the fluid flow velocity causes an increase in the shear stress acting on the wall and thus causes both the viscous sublayer to be replaced by a turbulent layer and also causes a reduction in the thickness of the thermal boundary layer. Because the thermal boundary layer is considered to be the main source of thermal resistance between the heated surface and the bulk of the coolant, it follows that when the thermal boundary layer is thinner, this enables more efficient heat transfer from the surface to the fluid. Lowering the viscosity of the fluid as a result of increasing the Reynolds number results in turbulence-induced macro-mixing. The presence of this increased turbulence means that there is a continual transfer of cooler fluid from the channel's core to the heated walls, which causes an increase in the temperature gradient at the interface between the solid wall and fluid. Since the heat transfer coefficient is directly related to this temperature gradient, the result of having both an increased temperature gradient along with reduced thermal resistance from the boundary layer gives rise to the maximum thermal performance at maximum flow rates.

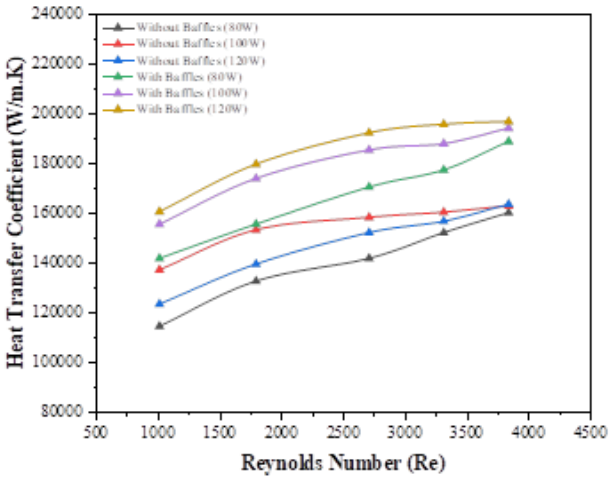

Figure 10. The heat transfer coefficients of baffled and unbaffled configurations of heat sinks as a function of Reynolds Number and across different power levels.

3.4. Comprehensive Performance

The thermal and hydraulic processes in terms of heat and hydraulic loss were compared by calculating the profit factor (J) as a function of the pumping power. Results demonstrate that as flow velocity increases, the profit factor decreases because a lower pumping power has the highest possible thermal-hydraulic efficiency of the heating element. Within the comparison of configurations, the comparison was between an unbaffled heat sink and a baffled heat sink. The unbaffled heat sink showed the greatest thermal-hydraulic efficiency. For example, at a heat input of 100 W and a pumping power of 0.14 W, the unbaffled heat sink produced a profit factor of 720, whereas the baffled heat sink produced a profit factor of only 480. This difference was due to the increased aerodynamic drag created by the solid baffles, which caused a larger hydraulic penalty for the baffled heat sink. Therefore, although the baffled heat sink provided a higher coefficient of heat transfer, improvements to the geometry of the baffles through openings or different attack angles would help reduce the hydraulic penalty associated with the baffled design and improve the profit factor for applications requiring a low energy use.

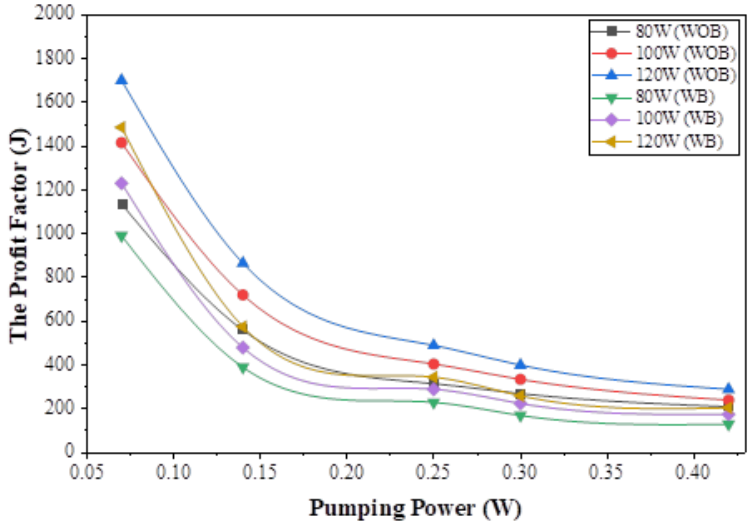

Figure 11. Profit factor curve for PFHS at different heat inputs with and without baffles.

4.4 Validation of Numerical Simulation Results

The results of the testing of the numerical simulation against those of an experiment proved to be reliable, as indicated by the validation process used to determine the simulator's reliability through the use of Computational Fluid Dynamics (CFD) analysis and validation with experimental data. The simulation was based on the unstructured tetrahedral mesh that was detailed earlier and used for solving steady-state conjugate heat transfer for numerical analysis. The total thermal resistance (Rth) was used as a measurement for the experimental and numerical testing for the representative test case (input power = 100 W, Re = 1800), with an experimentally measured thermal resistance of 0.171 K/W versus a CFD predicted thermal resistance of 0.179 K/W; this comparison produced a relative percentage deviation of approximately 4.75% from the experimental value.

The small discrepancy between numerical and experimental results is due to three main reasons. First, the CFD model contains Boundary Condition Assumptions that assume perfect thermal insulation of the duct walls, while in reality there are small losses (both in the form of conduction and radiative) to the surrounding environment. Second, the numerical model assumes perfect thermal contact between the heater and the heat sink; however, in reality, there is always some finite contact resistance between these two surfaces. Lastly, due to measurement uncertainty, both the total combined uncertainty (4.75%) of all instruments used to collect data and the simulation error overlap with each other, leading to the fact that the numerical data generated from the numerical model lies within the experimental confidence interval. When looking at literature on comparisons of numerical and experimental modeling results, the percent deviation of the CFD experimental data compared to the CFD numerical model aligns with the findings of previous authors; an example being Ma et al. (2020) who reported a 5.2% deviation in their experimental data, which further supports that the current CFD model provides accurate predictions of heat transfer performance in this study.

4.4.2. Assessment of Turbulence Modeling and Near-Wall Physics

To correctly resolve the thermal boundary layer, the near-wall mesh sizing was created so that the non-dimensional wall distance (y+) was maintained within the logarithmic region (30<y+<300). In addition, the use of Scalable Wall Functions with the standard K-Epsilon model helped to effectively model the viscous effects close to the fin surfaces. Although separating flows can often be complex and require the use of SST K-Omega models, preliminary testing has shown that the K-Epsilon model was able to produce good convergence results with only a 1.2% difference in the global heat transfer predictions when compared against higher order (K-Omega) models.

4.4.3 Qualitative Analysis of Temperature Distribution

The temperature distribution contours produced from our CFD modelling provide a qualitative perspective into how the baffling system in the PFHS cools down the heat module. Figures 13, 14, and 15 illustrate what the computational domain was like, along with the steady state temperature contours on the heatsink surface for an applied heat input value of 80W, 100W, and 120W.

Thermal Gradient Characteristics: The contours demonstrate that the highest temperature (red zones) occurs at the center of the heartsink's base, directly above the heat source. Heat is then carried upstream by conduction through the fins and disseminated to the environment by forced convection, with the temperatures gradually falling towards the leading and trailing edges of the fins (blue zones), providing evidence that convection has had the most influence along the airflow. Also of importance in the contours was the 'discontinuous' and 'waviness of the isotherms along the length of the fins. In a conventional unbaffled heatsink, the contours typically are smooth and parallel to one another, indicating a 'development phase' of the thermal boundary layer; however, Figures 14 and 15 have interruptions in their thermal boundary layer, indicating exactly where the baffle systems were located.

The outcome indicates that the transverse baffles function as efficient turbulence promoters by creating narrower pathways through which air can flow, accelerating the velocity of the local air (causing it to be similar to a jet) and causing the air to separate. On the other hand, the recirculation zones that form behind the baffles increase the mixing of the cooler thermal core fluid with the heated thermal layer surrounding the fin surfaces and limit the thickness of the thermal boundary layer, thus maintaining increased local heat transfer coefficients across the entire length of the heat sink, even when heat is applied at greater rates (120 Watts).

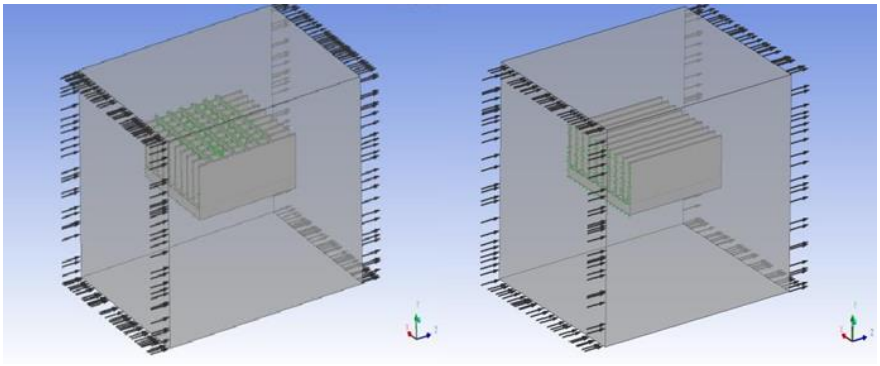

Figure 12. Heat sink in a wind tunnel using CFD simulation: (a) with baffles (b) without baffles.

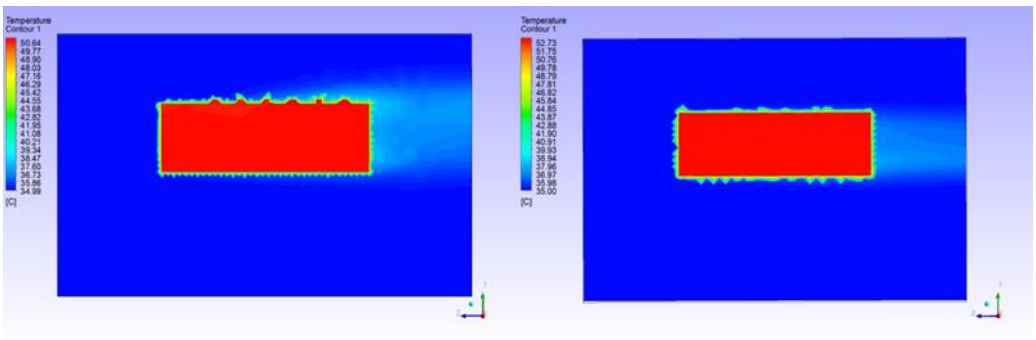

Figure 13. The heat sink's temperature distribution at 120 watts, with and without baffles.

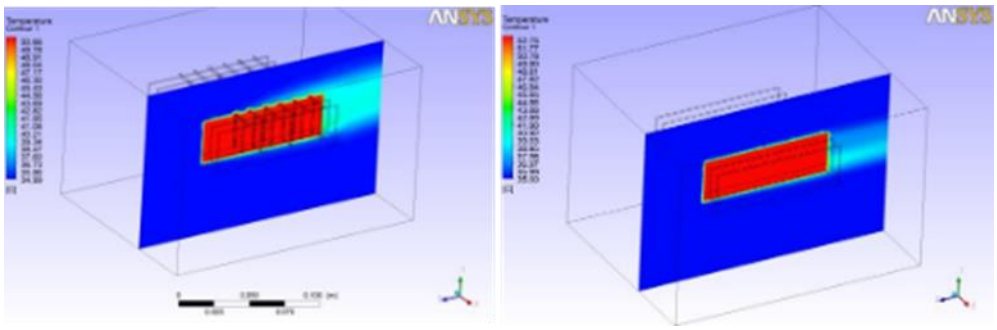

Figure 14. PFHS Mid-cut section of thermal field at 120 Watts (a) With baffles (b)Without baffles.

4. Conclusion

A comprehensive computer database study and a laboratory investigation into the thermal-hydraulic performance of a Plate Fin Heat Sink (PFHS) enhanced with two (2) cross (or transverse) copper baffles was conducted using the PFHS and examining the PFHS across a range of Reynolds numbers from 1,013 to a maximum of 38,000. This range included all the different heat loads between 80 W and 120 W that the PFHS experienced, allowing for the flow modulation potential of the system to enhance the heat sink's performance to be evaluated. Through validated numerical modelling, we found the PFHS's thermal performance predicted by the numerically modelled using the k-epsilon turbulence model was consistent with the laboratory thermal experimental data with an average deviation rate of only four percent from the actual Thermal Performance of PFHS. (4.75% deviation rate). The study shows that adding the baffles to the heat sink significantly disrupts the thermal boundary layer development and causes flow splitting. These findings suggest that, across all Reynolds numbers tested, using a baffled configuration reduces the thermal resistance of the heat sink by as much as 12.9% when compared to the unbaffled configuration. The study also demonstrates that baffles act as effective vortex generators for the flow and improve convective heat transfer performance by as much as 7.7%-8.9% Nusselt Number due to the additional vortex flow created from the baffles.

There was a direct relationship between the Reynolds Number and thermal performance in that higher flow velocities will decrease thermal resistance by decreasing the thickness of the viscous sublayer.

A hydraulic consequence of the enhanced thermal performance of a baffle design. Based on a Profit Factor analysis, it was determined that The Baffle Type Design provides improved cooling performance; however, the baffle type design experiences a significant loss in hydraulic head due to the presence of a barrier that partially obstructs airflow. The Unbaffled Type Design also has an increased energy efficiency ratio when pumping at a lower power due to this hydraulic loss from the baffles. Therefore, for applications where the maximum amount of heat transfer is required to be achieved in a limited space, and where the costs of additional energy for pumping are not a priority, it can be concluded that The Baffle Design is more advantageous. Future optimization efforts will be aimed at optimizing the baffle geometry to decrease the hydraulic loss associated with the baffle design, while still producing the large thermal performance benefits that have already been achieved.

References

[1] M. Sheikholeslami, M. Jafaryar, and Z. Li, “Second law analysis for nanofluid turbulent flow inside a circular duct in presence of twisted tape turbulators,” *J Mol Liq*, vol. 263, pp. 489–500, Aug. 2018, doi: 10.1016/j.molliq.2018.04.147.

[2] A. Dewan, P. Mahanta, K. Sumithra Raju, and P. Suresh Kumar, "Review of passive heat transfer augmentation techniques."

[3] K. Boukhadia, H. Ameur, D. Sahel, and M. Bozit, "Effect of the perforation design on the fluid flow and heat transfer characteristics of a plate fin heat exchanger," *International Journal of Thermal Sciences*, vol. 126, pp. 172–180, 2018, doi: https://doi.org/10.1016/j.ijthermalsci.2017.12.025.

[4] R. Akula, A. Gopinath, S. Rangarajan, and C. Balaji, "Experimental and numerical studies on heat transfer from a PCM based heat sink with baffles," *International Journal of Thermal Sciences*, vol. 159, p. 106525, 2021, [Online]. Available: https://api.semanticscholar.org/CorpusID:224924830

[5] M. S. Mahmud and E. Kabir, "Performance characteristics of a plate fin heat exchanger," 2020. [Online]. Available: https://api.semanticscholar.org/CorpusID:251395106

[6] L. N. Thanh, "The influence of baffled channel for cooling hot surface: Numerical simulation and Taguchi analysis," *Case Studies in Thermal Engineering*, 2023, [Online]. Available: https://api.semanticscholar.org/CorpusID:264396376

[7] R. Bouchenafa, R. Saim, S. Abboudi, and H. F. Oztop, "Effect of position and height of a shield on convective heat transfer performances of plate fin heat sink," *Int J Numer Methods Heat Fluid Flow*, vol. 25, pp. 1047–1063, 2015, [Online]. Available: https://api.semanticscholar.org/CorpusID:118945232

[8] S. Eiamsa-ard, A. Phila, K. Wongcharee, M. Pimsarn, N. Maruyama, and M. Hirota, "Thermal evaluation of flow channels with perforated-baffles," *Energy Reports*, 2023, [Online]. Available: https://api.semanticscholar.org/CorpusID:256221100

[9] K. Nakashima, T. Toda, M. Yoshida, S. Ishihara, and M. Yamamoto, "Development of Air-Cooled Cylinder Utilizing Baffle Plates between Fins with Cooling Ports," *SAE Technical Paper Series*, 2007, [Online]. Available: https://api.semanticscholar.org/CorpusID:131606830

[10] X. Cao, H. L. Liu, and X. dong Shao, "Heat transfer performance of a novel multi-baffle-type heat sink," *Entropy*, vol. 20, no. 12, Dec. 2018, doi: 10.3390/e20120979.

[11] H. Ameur, D. Sahel, and Y. Menni, "Numerical Investigation Of The Performance Of Perforated Baffles In A Plate-Fin Heat Exchanger," *Thermal Science*, vol. 25, no. 5 Part B, pp. 3629–3641, 2021, doi: 10.2298/TSCI190316090A.

[12] C. Kang and K.-S. Yang, "Heat Transfer Characteristics of Baffled Channel Flow," *Journal of Heat Transfer-transactions of The Asme*, vol. 133, p. 91901, 2011, [Online]. Available: https://api.semanticscholar.org/CorpusID:120876792

[13] A. Phila *et al.*, "Influence of notched baffles on aerothermal performance behaviors in a channel," *Case Studies in Thermal Engineering*, 2023, [Online]. Available: https://api.semanticscholar.org/CorpusID:258681808

[14] J. Hockaday and R. Law, "Enhancing Heat Transfer in Mini-Scale Liquid-Cooled Heat Sinks by Flow Oscillation—A Numerical Analysis," *Energies* , vol. 17, no. 11, Jun. 2024, doi: 10.3390/en17112459.

[15] Y. Menni *et al.*, "Computational fluid dynamic simulations and heat transfer characteristic comparisons of various arc-baffled channels," *Open Physics*, vol. 19, no. 1, pp. 51–60, Jan. 2021, doi: 10.1515/phys-2021-0005.

[16] S. S. Gore and A. S. Dhoble, "Server processor heat sink analysis and modifications to improve its thermal performance," *Mater Today Proc*, 2023, [Online]. Available: https://api.semanticscholar.org/CorpusID:256496767

[17] Y. L. Tsay, J.-C. Cheng, and Z. Zhan, "Enhancement of Cooling Performance of Block Heat Source Module in a Rectangular Channel by Installing Baffle onto Channel Wall," 2011. [Online]. Available: https://api.semanticscholar.org/CorpusID:107753597

[18] I. T'Jollyn, J. Rogiers, J. Nonneman, and M. De Paepe, "CFD simulation and geometric optimization of a novel baffle heat sink for power electronics cooling," in *Journal of Physics: Conference Series*, Institute of Physics, 2024. doi: 10.1088/1742-6596/2766/1/012175.

[19] R. Bakari, "Heat Transfer Optimization in Air Flat Plate Solar Collectors Integrated with Baffles," *Journal of Power and Energy Engineering*, vol. 06, pp. 70–84, 2018, [Online]. Available: https://api.semanticscholar.org/CorpusID:140043127